Lack of cadherins Celsr2 and Celsr3 impairs ependymal ciliogenesis, leading to fatal hydrocephalus

Fadel Tissir, Yibo Qu, Mireille Montcouquiol, Zhou Libing, Kouji Komatsu, Dongbo Shi, Toshihiko Fujimori, Jason Labeau, Donatienne Tyteca, Pierre Courtoy, et al.

Lack of cadherins Celsr2 and Celsr3 impairs ependymal ciliogenesis, leading to fatal hydrocephalus

Fadel TISSIR[1*], Yibo QU[1*], Mireille MONTCOUQUIOL[2], Libing ZHOU[1], Kouji KOMATSU[3,4], Dongbo SHI[4,5], Toshihiko FUJIMORI[3,4] , Jason LABEAU[1], Donatienne TYTECA[6], Pierre COURTOY[6], Yves POUMAY[7], Tadashi UEMURA[4,5], Andre M. GOFFINET[1]

[1]Université catholique de Louvain, Institute of Neuroscience, Developmental Neurobiology, B1200, Brussels, Belgium

[2]INSERM, U862, Neurocentre Magendie, Molecular Basis of Planar Polarity group, F-33000 Bordeaux, France

[3]Division of Embryology, National Institute for Basic Biology, Okazaki 444-8585 Aichi, Japan

[4]CREST, Japan Science and Technology Agency, Kawaguchi, Saitama 332-0012. Japan

[5]Graduate School of Biostudies, Kyoto University, Kyoto 606-8507, Japan

[6]Université catholique de Louvain, de Duve Institute, Cell Unit, B-1200 Brussels, Belgium

[7]Facultés universitaires Notre-Dame de la Paix, B-5000 Namur, Belgium

*These authors contribute equally to this work

Correspondence should be addressed to

fadel.tissir@uclouvain.be or *andre.goffinet@uclouvain.be*

Tel: +32 2 7647386

Fax: +32 2 7647385

Abstract

Ependymal cells form the epithelial lining of cerebral ventricles. Their apical surface is covered by cilia that beat coordinately to facilitate circulation of the cerebrospinal fluid. The genetic factors that govern the development and function of ependymal cilia remain poorly understood. Here we show that planar cell polarity cadherins Celsr2 and Celsr3 control these processes. In *Celsr2*-deficient mice, the development and planar organization of ependymal cilia are compromised, leading to defective cerebrospinal fluid dynamics and hydrocephalus. In double *Celsr2+3* mutant ependyma, ciliogenesis is dramatically impaired, resulting in lethal hydrocephalus. The membrane distribution of Vangl2 and Fzd3, two key planar cell polarity proteins, is disturbed in *Celsr2*, and even more so in *Celsr2+3* mutants. Our findings emphasize the role of planar cell polarity signaling in ependymal cilia development and function and in the pathophysiology of hydrocephalus, with possible implications in other ciliopathies.

Cilia are organelles that protrude from the apical surface of most eukaryotic cells. According to their structure and motility, they are classified into three groups[1]. Primary monocilia, present in most cells, lack a central pair of microtubules (9+0 structure), and play several roles in mechanosensation and cell signaling. Nodal cilia have a 9+0 structure but, unlike primary cilia, they move and generate an asymmetric distribution of morphogenetic cues in the node, thereby contributing to laterality[2]. The third group is composed of motile 9+2 cilia that cover epithelial cells lining airways, reproductive tracts, and cerebral ventricles. Motile cilia play crucial functions in clearing mucus and debris in the airways and may assist the transit of sperm and eggs in genital tracts[3-4]. In the early postnatal mammalian brain, neuroepithelial cells that line the cerebral ventricles leave the cell cycle and differentiate into a monolayer of ependymal cells. At the end of maturation, the apical surface of ependymal cells bears dozens of cilia that beat in coordinate manner to facilitate the circulation of the cerebrospinal fluid (CSF), from sites of production in choroid plexuses to sites of absorption in subarachnoid spaces. In mice, mutations in genes involved in the assembly or structure of ependymal cilia, such as *Mdnah5*[5], *Ift88* (also known as *Tg737* or *Polaris*)[6], and *Hy3*[7-8] affect cilia genesis, CSF dynamics, and result in hydrocephalus. Thus far, however, little is known about the genetic factors that govern ependymal cilia polarization and the relationship between the polarity and the development and function of these organelles.

Planar cell polarity (PCP), also known as tissue polarity, controls the polarization of epithelial cells in a plane perpendicular to their apicobasal axis. It was initially described in *Drosophila*, where it affects the stereotypic arrangement of cuticular hairs, sensory bristles, and ommatidia, through the control of so-called “core PCP genes” that include *Van Gogh*, *Frizzled*, *Flamingo* (also known as *Starry Night*), *Dishevelled*, *Diego*, and *Prickle*[9-10]. In mammals, PCP designates processes that control the development of polarized cellular structures and involve at least one core PCP gene ortholog[11]. PCP-dependent events include neural tube closure[12-13], hair bundle orientation in inner ear cells[13-14], and hair follicle patterning in the skin[15-17]. PCP-like mechanisms are also implicated in dendrite morphogenesis[18], and axon guidance[19-20]. In the

ciliated epidermis of larval *Xenopus,* morpholino downregulation experiments showed that *Dishevelled1-3, Inturned, and Fuzzy* are implicated in the control of the actin cytoskeleton and apical docking of ciliary basal bodies and that the planar orientation of multiciliate cells is disrupted when Disheveled, Vangl2 and Fuzzy signaling are altered[21-22], indicating a link between PCP signaling and ciliogenesis.

In the present work, we studied mice with inactivation of *Celsr2* and *Celsr3*, murine orthologs of the Drosophila core PCP gene *Flamingo,* and show that deficiency of these two seven-pass transmembrane cadherins dramatically disrupts the genesis of ependymal cilia, as well as the cellular partition of PCP proteins Vangl2 and Fzd3, leading to lethal hydrocephalus.

Results

Characterization of the *Celsr2* mutant

We described previously conditional and constitutive Celsr3 mutant mice [23]. The mutant *Celsr2* allele was generated by insertion of a targeting vector containing an internal ribosomal entry site (IRES) and the LacZ gene, into exon 23 of the *Celsr2* gene, preserving the endogenous splice acceptor (**Supplementary Fig. 1a**, **b**). RT-PCR and sequencing showed that the *Celsr2* transcript (Genbank 114050894) was interrupted at nucleotide 7107 and extended by the IRES-LacZ-neo sequence (**Supplementary Table 1**; see also the partial sequence of the recombinant cDNA in **Supplementary text**). If any truncated protein is produced, it should lack all transmembrane segments encoded by nucleotides 7123-7851, as well as the cytoplasmic tail (nucleotides 7852-8763). We analyzed neonatal brain extracts from wildtype (WT), mutant and heterozygous mice by western blot using an anti-Celsr2 antibody[24] and an antibody against beta-galactosidase. The anti-Celsr2 antibody detected a high molecular weight band in WT tissue. This band was less intense in extracts from heterozygous, and absent in those from homozygous animals, whereas the beta-galactosidase protein was present in heterozygous and homozygous mutant, but not WT extracts, confirming expression of the LacZ instead of *Celsr2* (**Supplementary Fig. 1c**).

Using the knocked-in beta-galactosidase reporter, we monitored the expression of Celsr2 in heterozygous mice. Consistent with published data[24-26], *Celsr2* expression was detected in all brain areas, from E11.5 to P5 (**Fig. 1a**–**h**).

Celsr2 mutant mice develop progressive hydrocephalus

Celsr2 mutant mice were viable and fertile, except for some females that had vaginal atresia. At birth, their brain did not display any flagrant morphological abnormality, suggesting that Celsr2 is not critical for cerebral embryonic development. However, a progressive ventricular dilation appeared between P5 and P10 with variable severity between animals, and became evident at P21 (**Fig. 2a**,**b**). The lateral ventricles were enlarged, and the septum had an abnormal triangular shape, due to

reduction of the dorsal part of the lateral septum. We did not observe any stenosis or constriction at the level of the foramen of Monro or of the aqueduct. The subcommissural organ (SCO), a structure thought to play a role in non-communicating hydrocephalus, was normal and synthesized the SCO-Spondin, a component of Reissner's fibers (**Supplementary Fig. 2**). Abnormalities in choroid plexus (ChP) can lead to hydrocephalus[6]. To check whether Celsr2 could be involved in the development of ChP, we analyzed its expression by beta-gal staining at different time points and did not detect any signal in ChP (**Fig. 1e**–**g**,**k**). We examined the ChP by transmission electron microscopy (TEM), and immunofluorescencce with acetylated tubulin antibodies, and did not find any difference between *Celsr2* mutants and control littermates (**Supplementary Fig. 3**).

In sharp contrast to ChP, *Celsr2* expression was very high in cells lining all cerebral ventricles, and the central canal of the spinal cord (**Fig. 1g**–**j** arrows), which differentiate into ependymal cells. To assess whether loss of Celsr2 function affects ependymal differentiation, we examined ependymal markers S100, CD24, and vimentin by immunofluorescence (**Fig. 3** and **Supplementary Fig. 4**)[27-29]. At P0, none of the three markers was expressed in cells in the ventricular zone destined to form the prospective ependymal layer. At P5, we detected S100, CD24 and vimentin immunoreactivity in ependymal cells lining the septal ventricular surface in control (**Supplementary Fig. 4a**,**c**,**e**), and *Celsr2*-deficient samples (**Supplementary Fig. 4a'**,**c'**,**e'**). At P10 and P21, we found S100 and CD24 in ependymal cells all around lateral ventricles (i.e. septal, striatal and cortical surfaces), and no difference was seen between controls and *Celsr2–/–* mutants (**Fig. 3a**–**b**,**d**–**e**, **Supplementary Fig. 4b**,**b'**,**d**,**d'**). Similarly, vimentin was expressed in ependymal cells and, even though the signal was higher in *Celsr2* mutant mice than in controls, no difference in the number of the vimentin positive cells was observed (**Fig. 3g**–**h ; Supplementary Fig. 4f**,**f'**). These results rule out the possibility that hydrocephalus may be due to defective differentiation of ependymal cells in *Celsr2* deficient mice.

Migration of young neurons, generated in the subependymal zone (SEZ) of the mature brain, was shown to depend on cerebrospinal fluid flow and is affected in hydrocephalic mice *Tg737*[30]. To

study the relationship between hydrocephalus and neurogenesis in the SEZ, we performed immunofluorescence using doublecortin (Dcx, a marker of neuroblasts - A cells), and GFAP (a marker of B1 cells)[27-29]. We found that Dcx and GFAP labeling was slightly higher in *Celsr2* mutant mice than in controls (**Supplementary Fig. 4g**–**g'**,**h**–**h'**).

Ciliary defects in *Celsr2* mutant mice

Since *Celsr2* was highly expressed in the ependymal layer (**Fig. 1d**–**g**), and impaired cilia function is a prevalent cause of hydrocephalus[6-7], we investigated ependymal cilia at P21 in lateral ventricles by double staining with the cilia marker acetylated alpha tubulin and ependymal markers S100, CD24 and vimentin (**Fig. 3**). Compared to WT, the number of cilia and ciliary tufts was clearly reduced in *Celsr2*$^{-/-}$ mice in which many ependymal cells labeled by S100, CD24 or vimentin had shorter and/or fewer cilia (**Fig. 3** arrowheads), and sometimes no cilia at all (**Fig.3** arrows).

These results indicate that some cilia fail to form, or form normally and then degenerate in *Celsr2* deficient mice. To distinguish between these possibilities, we studied cilia development at different stages with scanning electron microscopy (SEM) (**Fig. 4**). In newborn (P0) WT animals, only one primary cilium was found (**Fig. 4a**). Tufts of cilia appeared around P5, and increased gradually in number, in a caudal to rostral gradient, during the first postnatal week (**Fig. 4b**,**c**), to reach their mature density at P10 (**Fig. 4d**)[31]. At this stage already, fewer cilia tufts were found in *Celsr2*$^{-/-}$ (**Fig. 4e**) than in WT. Some mutant cells had stunted cilia (**Fig. 4e**, arrows), and others had reduced number of cilia (arrowheads). At the end of maturation (P21), cilia abnormalities were arresting. Whereas the mean number of cilia tufts was 15.8/mm^2**,** and all pointed approximately in the same direction in WT mice (**Fig. 4j**), the density of cilia tufts dropped to 6.7/mm^2 in *Celsr2* deficient mice, and their orientation was less uniform, with tufts from adjacent cells occasionally pointing to opposite directions (**Fig. 4k**). To quantify variations in cilia tufts orientation, we used SEM montages and plotted mean tuft orientation in cells with clearly identifiable tufts located in comparable areas of lateral ventricles in WT (439 cells) and *Celsr2* mutant mice (464 cells). The mean orientation was

arbitrarily set to zero. Using circular statistics (Oriana program) we found that mutant ependymal cells had a wider distribution of tufts orientations than the WT ($p<0.001$, Watson U^2 test; **Fig. 4l,m**). Taken together, these results show that cilia fail to form normally in *Celsr2* mutant mice, and that residual cilia tufts display abnormal organizations at the end of maturation.

Celsr2 mutation affects cilia at the single cell level

To study effects of *Celsr2* inactivation on cilia development at the individual cell level, we used TEM in sections cut tangentially to the surface of the lateral ventricle, and examined the orientation of basal feet. These structures extend laterally to basal bodies, point to the effective stroke of cilia beats[32-33] and are considered a landmark of cilia polarity[34]. In WT (**Fig. 5a**), only 8.5% of basal feet exhibited divergent orientation with respect to their neighbors (82 basal feet from 15 cells were examined; in 10 cells, all basal feet had uniform orientation; in the 5 others, 1 or 2 basal feet/per cell exhibited divergent orientation). In *Celsr2* mutant cells (**Fig. 5b**), 31.8% of the basal feet deviated from the common orientation (47 out of 148 basal feet examined in 14 cells; each cell had at least one basal foot with divergent orientation). Inasmuch as some mutant cilia degenerated prematurely or did not develop at all (**Fig. 5e**) and were thus not considered, the disorganization of basal feet in *Celsr2* mutants is most probably underestimated.

During assembly of motile cilia, basal bodies (bb) form deep in the cytoplasm and are transported to the apical surface via actin-dependent mechanisms[33, 35-36]. To study how *Celsr2* inactivation influences ependymal ciliogenesis, we performed sections perpendicular to the ventricular surface to examine by TEM the position of bb relatively to the apical surface of ependymal cells at P10. In WT samples, bb formed a single row just beneath the apical surface (**Fig. 5d**). By contrast, procentrioles and bb, together with densely osmiophilic profiles that probably correspond to deuterosomes, were found at deeper, more basal levels in *Celsr2* mutant cells (arrowheads in **Fig. 5e**). To quantify these differences, we measured the distance between bb and the apical surface and calculated the proportion of embedded bb (defined as bb located below the first

row, more than 500 nm from the surface). In *Celsr2*$^{-/-}$, 54 % of bb were embedded versus 5% in WT (**Fig. 5g**; X^2 test, $p < 0.001$). Most embedded bb were not associated with ciliary shafts. However, fully formed cilia were occasionally seen deep in the cytoplasm (**Fig. 5h**). Presumably, ectopic cilia and embedded bb are fated to premature degeneration, which may account for the reduced density of cilia in adult *Celsr2* mutant ependymal cells.

Celsr2 mutation impairs cilia function

In rodents, mutations that affect cilia motility lead to hydrocephalus[5-8, 37]. The ultrastructure of residual *Celsr2* mutant cilia were unremarkable and displayed the typical "9+2" structure of motile cilia (**Supplementary Fig. 5**). This indicated that *Celsr2* mutation has no direct effect on the axoneme structure and raised the question of the motility of cilia in *Celsr2* mutants. To investigate this, we prepared brain slices from 12 days-old animals and recorded cilia movement with a high speed camera. We found two classes of movement in WT. One movement is more dynamic than the other, and reminiscent of "seaweeds" drifted by restless waves. The other is a smaller motion that resembles a "wiggling pigeon's neck". Both classes were found in *Celsr2* mutant cells that harbored intact cilia, suggesting that cilia movements were not grossly affected by Celsr2 deficiency (**Supplementary Movies S1-4**).

Could the reduced number of cilia and cilia tufts result in inefficient CSF dynamics despite the preserved cilia beat at the single cell level? To address this question, we studied the flow generated by cilia beats in lateral ventricles in vibratome slices, from P0 to P21. Ependymal cilia were beating from P5 onwards, but they generated a significant flow only from P8. When latex beads were added to the medium of WT slices at P7-P10 (**Fig. 6a**, n = 13), their movement, tracked as described in Methods, was consistently directed from the caudal to the rostral pole of the lateral ventricles, with a mean bead velocity of 78.3 ± 35.6 (SD) µm/s. In *Celsr2* deficient slices (Fig 6b, n = 19), the overall movement of beads was slower and less clearly directed towards the rostral pole than in WT, and the mean bead velocity was 26.6 ± 9.7 (SD) µm/s. Frequently, beads exhibited a

circling movement without any clear resultant displacement along the rostrocaudal axis (**Supplementary Movie S5**). Both directions and velocities, compared respectively using Watson U^2 (**Supplementary Table S2**) and student's t-test (**Fig. 6d**), were significantly different in the two genotypes. Although the size of the ventricle could affect the speed of beads movement, our data indicate that inactivation of *Celsr2* impairs the efficiency of cilia beats, which could compromise CSF dynamics and thereby contribute to hydrocephalus.

Celsr2 and *3* have redundant functions in ciliogenesis

Celsr3 expression is not detected in ventricular zones during embryonic development (**Fig. 7a**,**b**)[24-25], but is initiated postnatally in cells lining lateral ventricles, when they become postmitotic and start differentiating into ependymal cells (**Fig. 7c**,**d**)[25]. We have evidence that *Celsr2* and *Celsr3* have redundant functions in neuronal migration and axon guidance, suggesting that they may similarly cooperate in ependymal ciliogenesis. To test this possibility, we studied ependymal cells of lateral ventricles in double *Celsr2* and *Celsr3* mice. Constitutive *Celsr3* mutant mice die at P0[19]. Therefore, we produced Celsr3|Emx1 mice, in which *Celsr3* is inactivated in dorsal telencephalon, including the ependymal layer in the roof of lateral ventricles[23]. In these mice, referred to as "*Celsr3"*, cilia were indistinguishable from that in WT cells (Compare **Fig. 4d** with **4f**). The density of cilia tufts was 15.6/mm^2, versus 15.8/mm^2 for the WT, further confirming that mutation of *Celsr3* alone did not perturb ependymal cilia development. However, when regional *Celsr3* inactivation was combined with deficiency of *Celsr2* in [*Celsr2*$^{-/-}$*; Celsr3|Emx1*] mice, referred to as "*Celsr2+3*", a severe hydrocephalus appeared from P5. Lesions were much more important than in *Celsr2* mutant animals (**Fig. 2**, compare **b** with **c**). Even though *Celsr3* is ablated only in *Emx1* expressing ependyma, this led to extreme thinning of the cerebral cortex, with formation of a discontinuity in the dorsal hemisphere, and death of animals around weaning time (**Fig 7e**–**f**). The number of Dcx and GFAP positive cells was higher in *Celsr2+3* mutants than in controls (**Supplementary Fig. 4g**,**h**,**g"**,**h"**). Immunofluorescence analysis of S100, CD24 and vimentin indicated that ependymal cells differentiate normally (**Supplementary Fig. 4a"**,**b"**,**c"**,**d"**,**e"**,**f"**), and persist in the mature mutant

brain (**Fig. 3c**,**f**,**i**), although their shape was stretched and some cells may have degenerated because of increased pressure, as reflected by vimentin immunoreactivity (**Fig. 3i).** Large areas of dorsal lateral ventricles were completely devoid of cilia (**Fig. 4g**–**i**), preventing any accurate estimation of cilia tufts density. These cilia-free zones persisted until death, indicating defective rather than delayed ciliogenesis. In cells with residual cilia, the percentage of basal feet with abnormal orientation reached 43.16% (60 of 139 scored basal feet) (**Fig. 5c**). These abnormalities were comparable to those reported in mice with defective cilia motility, such as Hydin deficient mice[7]. 70% of the bb were embedded in the basal cytoplasm (**Fig. 5f**,**g**). Ectopic cilia had a tilted configuration and their tips were not oriented apically, contrasting with the upright alignment of apical cilia in WT and ectopic cilia in *Celsr2* mutant cells (**Fig. 5i**). When latex beads were added to freshly prepared brain slices from *Celsr2+3* mice (**Fig. 6c**, n = 2), they drifted very slowly along different directions in the enlarged ventricle, with an estimated velocity of 13.0 ± 4.2 (SD) µm/s versus 78.3 ± 35.6 (SD) µm/s for the WT. This difference was statistically significant using the Watson U^2 test (**Supplementary Table S2**) and student's t-test (**Fig. 6d**).

Emx1-Cre is expressed not only in ependyma but also in cortical glutamatergic neurons and glial cells. To ascertain that the effects observed were due to Celsr3 deficiency in ependyma, we produced double mutant [*Celsr2*$^{-/-}$*; Celsr3|Nex*] mice, in which *Celsr3* is inactivated in cortical neurons but not in ependyma[38]. Brains of these mice were indistinguishable from those in *Celsr2*$^{-/-}$ animals (n = 5), demonstrating that the contribution of *Celsr3* is most likely due to its expression in ependymal cells.

Fzd3 and Vangl2 distribution is altered in *Celsr* mutants

Studies in the skin showed that PCP signaling play essential roles in hair follicle polarization and orientation[15-17]. Celsr1 and Vangl2 form physical complexes *in vitro* , and Celsr1 is required for the correct targeting of Vangl2 and Fzd6 to the plasma membrane[17]. To gain insight into the mechanisms of action of Celsr2 and Celsr3, and assess whether their function could indeed be mediated by PCP,

we studied the distribution of Fzd3 and Vangl2, two key components of the PCP pathway expressed in ependymal cell precursors[14, 39-40] (**Fig. 8**). In WT at P5, Fzd3 and Vangl2 signals displayed polygonal patterns, restricted to the lateral membrane, with a continuous (Fzd3) or punctuate distribution (Vangl2) (**Fig. 8a**,**d**). In *Celsr2*$^{-/-}$ tissue, Fzd3 and especially Vangl2 were only partially targeted to the cell membrane. Rather, more signal was associated with intracellular vesicles (**Fig. 8b**,**e**). In *Cels2+3* double mutants, the impaired distribution of Fzd3 was even more evident, whereas Vangl2 was downregulated (**Fig. 8c**,**f**). The restricted polygonal pattern upon labeling of the junctional protein ZO–1 was fully preserved in *Celsr2* and *Celsr2+3* mutants, showing that the abnormal distribution of Vangl2 and Fzd3 was not secondary to defective junction organization (**Supplementary Fig. 6**).

Discussion

Using *in vivo* approaches in mice, we show that *Celsr2* and *Celsr3*, two murine orthologs of the core PCP gene *Flamingo* in *Drosophila*, are key regulators of ciliogenesis in the ependyma, and that their inactivation leads to lethal hydrocephalus. In *Celsr2* and *Celsr2+3* mutant ependyma, cilia never develop in normal numbers and display abnormalities in their morphology, position, and planar organization. Ciliary basal feet are disoriented, and basal bodies and cilia assemble ectopically deep in the cytoplasm. These defects do not primarily affect cilia motility; yet they alter ependymal function, leading to ventricular dilation. The lateral plasma membrane localization of Vangl2 and Frizzled3, two established PCP proteins, is disrupted in ependymal cells precursors in *Celsr2* and *Celsr2+3* mutant mice, providing strong indication that Celsr2 and Celsr3 regulate ciliogenesis via PCP signaling.

Previous studies in frog larval epidermal cells provided the first evidence of a link between PCP and cilia development. In these cells, morpholino knockdown of *Inturned*, *Fuzzy* and *Disheveled1-3* affect cilia polarity and ciliogenesis, by preventing normal docking of basal bodies to the apical cytoplasm[21-22]. Although these elegant studies indicate a relationship between ciliogenesis and PCP signaling, it is worth mentioning that *Inturned* and *Fuzzy* are not considered *bona fide* core PCP genes, and that, besides PCP, *Disheveled1-3* also regulate canonical and non canonical Wnt signalings. Moreover, being near tetraploid, *Xenopus laevis* cells may express additional PCP gene orthologs than those that are identified in *Xenopus tropicalis* and whose sequences are used for morpholino design. In mice, mutations in genes encoding proteins implicated in cilia structure or development, such as *Bbs1*, *Bbs4* and *Ift888*, affect the “V shaped” orientation of actin stereocilia bundles at the surface of inner ear cells, an organization that is governed by the directed growth of a monocilium during development[39, 41]. This phenotypic trait is typically found in mice with mutations in PCP genes *Celsr1*, *Frizzled3*, *Frizzled6* and *Vangl2*[11, 13-14]. Furthermore, conditional inactivation of the ciliary gene *Kif3a* in neural progenitors and radial glia affects ciliary basal feet orientation and planar polarity of ependymal cells[42]. These data suggest that the link between PCP and ciliogenesis,

described in amphibian epidermal cells, is conserved in mammals. Our observations that core PCP genes *Celsr2* and *Celsr3* are essential for the correct positioning of cilia at the apical surface of ependymal cells, for cilia function as well as for CSF dynamics, further extend and clarify this view.

Presumably, PCP signals act on the cytoskeletal machinery required to assemble cilia at the cell surface, a mechanism highly reminiscent of that involved in the growth of the actin shaft of hairs in *Drosophila* wing cells[43]. That PCP signaling acts upstream from cilium assembly is also supported by observations that PCP proteins are normally distributed in cochlear cells in mice with mutation of the "ciliary gene" *Ift888*[39]. Factors that regulate apical basal body docking remain poorly understood. Our observation that cilia can form deep in the cytoplasm in *Celsr2* and *Celsr2+3* mutant ependymal cells and that ectopic basal bodies can still serve as seeds for cilia formation, indicates that apical docking is not absolutely required for cilia assembly *per se*. Studies of ciliogenesis in the quail oviduct showed that localization of basal bodies to the apical cell domain depends on actin dynamics[35]. In line with this, ciliogenesis is defective in *Foxj1* mutant mice, due to abnormal basal body anchoring to the actin-based apical cytoskeleton, and failure of RhoA-mediated apical actin enrichment[44-47]. The hypothesis that PCP signaling regulates apical actin network formation required for docking of basal bodies and normal ciliogenesis predicts that mutations in other genes that control PCP in mice should similarly lead to cilia dysfunction and hydrocephalus. Unfortunately, unlike *Celsr2* mutants, mice with mutations in other PCP genes, such as *Celsr1*[13], *Frizzled3* and *6*[40], *Vangl2*[12] all die perinatally, before ependymal cilia develop. The generation of conditional mutant mice for PCP gene orthologs would provide additional tools to address these issues. In addition to defective docking, we also find impairment of the planar organization of cilia tufts in mature *Celsr* mutant ependymal layers. This phenotype could reflect a direct effect of Celsr mutations, but it may also be a consequence of disturbed CSF flow[34] in these hydrocephalic mice.

Finally, our findings underscore the role of PCP signaling in ependymal function and hydrocephalus. In man, CSF flow is commonly ascribed to a pressure gradient generated by blood pulsations, between the sites of production and absorption. In contrast to rodents, cilia beats are usually not considered a key determinant of human CSF dynamics, nor a relevant pathophysiological factor of hydrocephalus[48]. Our results add to a growing body of evidence that the impact of cilia on CSF dynamics is extremely important in rodents and probably not negligible in man, and invite additional scrutiny of ependyma and cilia function in patients with communicating hydrocephalus. Abnormalities of cilia are also associated with cystic pathology in the kidney, liver and pancreas[1, 49]. PCP genes such as *Celsr1-2, Disheveled1-2, Frizzled3, Vangl1-2* are expressed in these organs[24, 50], suggesting that PCP might be involved in the polarity and function of their cilia, both in normal and pathological conditions.

Acknowledgements: We wish to thank Kevin Jones for Emx1-Cre mice, Gundela Meyer for providing the Anti SCO-spondin antibody, and Klaus-Armin Nave for NEX-Cre mice. We also thank, Valérie Bonte, Isabelle Lambermont and Esther Paitre for technical assistance, and Marie France Boulanger, Yves Houbion, Marie-Jeanne Vertez and Renaud Vigneron for help with electron microscopy. This work was supported by grants from the Actions de Recherches Concertées (ARC-186), FRFC 2.4504.01, FRSM 3.4501.07, Interuniversity Poles of Attraction (SSTC, PAI p6/20), the Fondation médicale Reine Elisabeth, the Wallonne and Bruxelloise régions from Belgium; and from the Japan Science and Technology Corporation (CREST). F.T. is research associate at the Belgian FNRS.

Author's contribution: F.T. characterized the *Celsr2* mutant allele, studied Celsr2 and Celsr3 expression, and carried out histological and immunofluorescence studies; Y.Q. performed SEM and TEM with the help of Y.P; L.Z. and J. L. studied cilia function in brain slices; K.K. monitored cilia beats and analyzed data with S.D. and T.F.; M.M. provided the Vangl2 antibody and commented on the manuscript; D.T. and P.C. helped with the confocal microscopy and commented on the manuscript. T.U. analyzed the ciliary beat data, provided the Celsr2 antibody and commented on the manuscript. F.T. and A.M.G. designed research, analyzed data and wrote the manuscript. Authors declare no conflict of interest.

Methods

Mutant mice. All animal procedures were carried out in accord with European guidelines and approved by the animal ethics committee of the Université catholique de Louvain. The Celsr2 mutant allele (Celsr2^{tm1Dgen}) was generated by Deltagen and *Celsr2* heterozygous mutant mice were obtained from the Jackson laboratory. Celsr3 and Celsr1 mutants were described previously [23]

RT-PCR. Total RNA was extracted using NucleoSpin® RNA II kit (Macherey-Nagel) and converted to single-stranded cDNA using the ImProm-II reverse transcriptase (Promega) with random primer (0.5 µg/ml) in 20 µl of 1X ImProm-II buffer (6 mM MgCl2, 0.5 mM each dNTP, and 2 U recombinant RNasin ribonuclease inhibitor). For subsequent PCR amplification, cDNA samples were incubated with 500 nM of each of the sense and antisense primers and 1 unit of recombinant Go Taq polymerase (Promega) in 20 µl of 1X PCR buffer.

Beta-galactosidase staining. Animals were perfused with 2% paraformaldehyde, 0.1% glutaraldehyde in PBS. Dissected brains were postfixed for 1 hour at room temperature, sliced using a vibratome and stained with a solution containing 1mg/ml X-gal, 5 mM $K_3Fe(CN)_6$, 5mM$K_4Fe(CN)_6$, 2mM $MgCl_2$ in PBS.

Western blot, histology and immunohistochemistry. For western blots, we used mouse anti- beta-galactosidase (1:200, Hybridoma Bank) and mouse anti-Celsr2 (supernatant, [24]. For histological examination, 8µm-thick paraffin sections were stained with cresyl violet or hematoxylin eosin (HE). For immunohistochemistry, we used 10 µm-thick sections or 100 µm thick-vibratome slices with the following primary antibodies, rabbit anti SCO-spondin (1:1000, gift from G. Meyer & E.M. Rodriguez), rabbit anti-S100 (1:500, DakoCytomation), mouse anti-actylated alpha tubulin (1:2500, Sigma), mouse anti-vimentin (1:1000, Sigma), rat anti-CD24 (1: 500, BD Pharmigen), rabbit anti-GFAP (1:500, Chemicon), rabbit anti-doublecortin (1:500, Cell signaling) goat anti-Fzd3 (1:25, R&D), rabbit anti-Vangl2 (1:500, M. Montcouquiol), rabbit anti-ZO–1 (1:100, Zymed). Secondary antibodies were goat anti-mouse-AlexaFluor488 and AlexaFluor568, goat anti-rabbit-AlexaFluor488

and AlexaFluor568, donkey anti-goat AlexaFluor488, and chicken anti-rat AlexaFluor488 (1:400, all from invitrogen). Immunofluorescence was performed using standard procedures; preparations were examined with a LSM510 confocal microscope (Zeiss).

Recording and analysis of cilia beats. Cilia were observed in freshly prepared, 300 µm thick vibratome sections at P7, P8 and P10. Sections were maintained in DMEM containing 20 mM HEPES in air as described[7], or in artificial cerebrospinal fluid (ACSF : NaCl 124mM, KCl 3mM, NaHCO3 26mM, CaCl2 2mM, MgSO4 1 mM, KH2PO4 1.25 mM, Glucose 25 mM and Hepes 10 mM, pH 7.4) under water-saturated 95% oxygen and 5% CO2. A maximum of 1 hour elapsed between sacrifice of animal and the end of observations, and both methods yielded similar results. 1µm micrometer latex beads (Sigma L2778) were added to medium prior to video recording. Movies were fragmented into individual images corresponding to 40 ms, and beads were tracked in selected frame series using the "Retrac 2" program to estimate speed and direction. Directions (30-40 tracks for each genotype) were compared using circular statistics, Watson U^2 test (Oriana program).

For high speed recording of individual cilia beats, we used a 100x objective and Nomarski optics. Movies were acquired at 200 frames/second using a digital high speed camera (HAS-220; Ditect Co., Ltd, Japan) and analyzed using Move-MN software (Library-inc., Japan).

Electron microscopy. Brains were fixed by perfusion of the animal under deep anesthesia, with 2.5% glutaraldehyde in phosphate or cacodylate buffer (0.1M, pH7.5), and postfixed for 1 hour in the same fixative. For SEM, 300-500 µm-thick horizontal slices containing the roof of the lateral ventricles were cut with a vibratome, dehydrated and prepared for observation using a Jeol 7500F scanning electron microscope. Blocs for TEM were rinsed, postfixed in osmium and embedded in epoxy resin. Thin sections were stained with uranyl acetate and lead citrate, and observed with a Philips Tecnai 10 transmission electron microscope.

Statistics. Circular statistics were carried out with the Oriana program, using the Watson U^2 test to compare dispersion of orientations. Bead velocities in brain slices experiments were compared using student's t-test. A "*p*" value inferior to 0.05 was considered significant.

Legends

Figure 1: *Celsr2* is expressed in differentiating ependymal cells but not in choroid plexus. Expression of *Celsr2* depicted by beta-galactosidase histochemistry in E11.5 embryo (**a**), and in brain coronal sections at E14.5 (**b**), E17.5 (**c**), P0 (**d**–**g**) and P5 (**h**). Widespread staining was observed in the central nervous system at E11.5, and in all brain regions, with highest levels in the layer lining cerebral ventricles at P0 (arrows in **d**–**g**). Note that no staining was found in choroid plexus (arrowheads in **b**–**d** and **h**). Scale bar: 100 µm in (**b**–**c**), 500 µm in (**d**–**h**).

Figure 2: *Celsr2* and *Celsr2+3* mutant mice display hydrocephalus. (**a**–**c**) Nissl-stained coronal sections from wild type (left), *Celsr2* (middle), and *Celsr2+3* (right) mice at P21. Combined inactivation of *Celsr2* and *Celsr3* in ependymal cells results in severe hydrocephalus and extreme thinning of the cerebral cortex and basal forebrain (**c**). Cx: cortex, LSd: dorsal part of lateral septum, LSv: ventral part of lateral septum, Sep: septum. Scale bar: 1mm.

Figure 3: Ependymal cilia abnormalities in *Celsr2* and *Celsr2+3* mutant mice. P21 brain sections were stained with DAPI (left), and by immunofluorescence for ependymal markers (second column) S100 (**a**-**c**), CD24 (**d**-**f**) and vimentin (**g**-**i**), and for acetylated alpha tubulin (third column). In *Celsr2* and *Celsr2+3* samples, ependymal cells display many ciliary defects, including shorter cilia and reduced number of cilia per cell (arrowheads), as well as absence of cilia (arrows). Scale bar: 20 µm

Figure 4: Ciliogenesis is altered in *Celsr2* and *Celsr2+3* deficient mice. (**a**–**k**). SEM micrographs of ependymal cells lining the roof of lateral ventricles at P0 (**a**, arrowheads show monocilia), P3 (**b**), P6 (**c**), P10 (**d**–**i**), and P21 (**j**,**k**). Cilia develop progressively after birth and reach maturity by P10. At this stage, the number of cilia tufts is reduced and cilia have many morphological abnormalities in *Celsr2* (**e**) and *Celsr2+3* (**g**–**i**) mutants as compared to WT (**d**) and *Celsr3* mutants (**f**). Arrows show shorter cilia, and arrowheads cilia tufts with reduced number of cilia. In the mature brain, individual cilia

converge to a common orientation in WT (arrows in **j**), but cilia tufts of mutant mice (**k**) are less regularly oriented and, in some cases, individual cilia in a given cell do not point to the same direction (asterisks). (**l**,**m**) dispersion of cilia tufts orientation around the mean in WT (**l**) and *Celsr2* mutant mice (**m**). Scale bars: 5µm (**a**,**j**,**k**), 10 µm (**d**–**f**, **h**–**i**), 20 µm (**b**,**c**), 100 µm (**g**).

Figure 5: Inactivation of *Celsr2* and *3* affects polarization and apical positioning of cilia. (**a**–**c**) TEM analysis of tangential sections of ependymal cells from WT (**a**), *Celsr2*, (**b**) and *Celsr2+3* animals (**c**). Arrows indicate the orientation of basal feet which display dispersed orientations in mutants. (**d**–**f**, **h**–**i**) Ependymal cells in radial sections, from WT (**d**), *Celsr2* (**e**, **h**) and *Celsr2+3* (**f**, **i**) mice. Arrows point to normally positioned basal bodies, arrowheads to embedded basal bodies, and double arrowheads to ectopic cilia. (**g**) Graph showing the proportion of basal bodies with abnormal apicobasal position. Scale bars: 500 nm (**a**, applies to **b**–**c**), 1 µm (**d**, applies to **e**,**f**,**h**,**i**).

Figure 6: *Celsr2* and *Celsr2+3* deficiency affects fluid flow. Latex beads were added to brain slices prepared from P8 mice and their movement in the lateral ventricle was recorded with a video camera. Movies were fragmented and sequential images were analyzed using the "Retrac 2" software. Each bead was tracked for 720 ms and the time between two dots is 40 ms. Circles indicate track end-points. In WT (**a**), bead motion was uniform and trajectories formed almost parallel lines. In *Celsr2* (**b**) and *Celsr2+3* (**c**) mutants, tracks were shorter than in the control, and beads moved in divergent directions (Watson U^2 test, $p<0.05$, **Supplementary Table S2**). The speed was calculated for each genotype and is shown as mean ± s.e.m in (**d**); $p < 0.0001$, ***. Scale bar: 20 µm

Figure 7: Combined mutation of *Celsr2* and *Celsr3* causes lethal hydrocephalus. (**a**–**d**) Coronal sections hybridized with *Celsr3* digoxigenin labeled probe. *Celsr3* is not expressed in the ventricular zones at E14.5 (**a**), but is turned on postnataly in cells of the prospective ependymal layer (**c**–**d**, arrowheads). Note the absence of *Celsr3* trasnscript in the

choroid plexus (arrows in **a**–**d**). (**e**) *Celsr2+3* mutant mice have a dome-like appearance of the head caused by hydrocephalus, and their brains (**f**) display extreme thinning of cerebral cortex and holes in telencephalic walls. VZ: ventricular zone, H: hippocampus, GE: ganglionic eminence, cc: corpus callosum, Str: striatum. Scale bar: 200 µm

Figure 8: The cellular distribution of Fzd3 and Vangl2 is perturbed in *Celsr2* and *Celsr2+3* mice. Confocal immunofluorescence imaging showing the cellular distribution of Fzd3 (**a**–**c**, horizontal sections in upper panels, and vertical sections in lower panels); and Vangl2 (**d**–**f**), in the ventricular zone at P5. The polygonal pattern that reflects localization of Fzd3 (**a**) and Vangl2 (**d**) at the lateral plasma membrane in normal mice (arrowheads) is modified in *Celsr2* (**b**,**e**) and *Celsr2+3* (**c**,**f**) mutants. The Z sections (rows 2 and 4) are at the level of red lines in horizontal sections (rows 1 and 3), which were recorded at the position of blue lines in vertical sections. Scale bars: 5 µm.

Supplementary Fig. 1: Targeted insertion of LacZ into *Celsr2* locus. (**a**) *Celsr2* has 34 exons (rectangles); arrows 1-9 indicate positions of primers used in RT-PCR (see **Supplementary Table S1**). (**b**) The IRES-LacZ-Neo cassette was inserted in exon 23 downstream from nucleotide 7102 (Genbank 114050894). (**c**) Western blot analysis of brain extracts from wild type, heterozygous, and homozygous brain. *Celsr2* (top) was present in wild type and heterozygotes, and replaced by beta galactosidase (bottom) in mutant mice.

Supplementary Fig. 2: The subcommissural organ (SCO) develops normally in *Celsr2* mutant mice. (**a**) Nissl stained coronal section at the level of the SCO at P10. (**b**,**c**) Sco-spondin immunofluorescence shows that the SCO synthesizes the glycoprotein SCO-spondin, which aggregates and forms the Reissner's fiber (arrowheads). V3: third ventricle. Scale bar : 100 µm.

Supplementary Fig. 3: Choroid plexus displays normal cilia in *Celsr2* and *Celsr2+3* mutant mice. Immunofluorescence for acetylated alpha tubulin reveals mono and grouped cilia on epithelial cells in choroid plexus. No difference was observed between WT (**a**), *Celsr2* (**b**), and *Celsr2+3* (**c**) mutants. Nuclei are counterstained with DAPI. Scale bar: 10 µm.

Supplementary Fig. 4: Ependymal cells differentiate normally in *Celsr2* and *Celsr2+3* mutant mice.

(**a**–**f”**): Immunofluorescence for S100 (**a**–**b”**), CD24 (**c**–**d”**) and vimentin (**e**–**f”**) show that ependymal cell lining lateral ventricles differentiate in similar ways in WT (**a**,**b**,**c**,**d**,**e**,**f**), *Celsr2* (**a’**,**b’**,**c’**,**d’**,**e’**,**f’**), and *Celsr2+3* (**a”**,**b”**,**c”**,**d”**,**e”**,**f”**) mutant mice.

(**g**–**h”**): Coronal sections of mature brain stained for Doublecortin (**g**–**g”**) and GFAP (**h**–**h”**). The number of Doublecortin and GFAP positive cells is increased in the subependymal layer of *Celsr2* (**g’**,**h’**) and *Celsr2+3* (**g”**,**h”**) mutants as compared to WT (**g**,**h**) mice.

(**i**–**k”**): Immature neurons, stained for doublecortin (DCX). Compared to WT (**i**,**j**,**k**), the number of DCX positive cells is increased in the subependymal niche of *Celsr2* (**i’**,**j’**,**k’**) and *Celsr2+3* (**i”**,**j”**,**k”**) mutant mice. Scale bar: 50 µm in (**c**–**c”**, **e**–**e”**, and **i**–**i”**), 100 µm for other panels

Supplementary Fig. 5: Ependymal cilia have normal ultrastructure.

TEM micrographs of cross sections of cilia from the WT (**a**), *Celsr2* (**b**) and *Celsr2+3* (**c**) mutant mice. Mutant cilia have the typical (9+2) structure of motile cilia. Scale bar: 100 nm

Supplementary Fig. 6: Normal distribution of ZO–1.

(**a**–**c**) immunofluorescence showing that the subcellular localisation of ZO–1 is preserved in *Celsr2* (**b**) and *Celsr2+3* (**c**) mutant ependyma. The Z sections (rows 2) are at the level of red lines in horizontal sections (rows 1). Scale bar: 5 µm

Supplementary Movies 1–4: Cilia beat exhibits two types of movements in the WT tissue, namely “seaweed” (**movie 1**) and “pigeon neck” (**movie 2**), and both are preserved in *Celsr2* deficient tissue (“seaweed”, movie 3; “pigeon neck”, movie 4). Images were acquired at 200 frames/s. The playback rate of each the movie is 50 frames/sec, and each movie is made of 150 frames.

Supplementary Movie 5: Movement of latex beads in lateral ventricle of WT and *Celsr2* mutant tissue. In contrast to WT where beads move from the caudal to rostral pole, there is no significant displacement of beads in the mutant. Images were acquired using a standard video camera, at 25

References

1. Davenport, J.R. & Yoder, B.K. An incredible decade for the primary cilium: a look at a once-forgotten organelle. *Am J Physiol Renal Physiol* **289**, F1159-1169 (2005).
2. Marshall, W.F. & Kintner, C. Cilia orientation and the fluid mechanics of development. *Curr Opin Cell Biol* **20**, 48-52 (2008).
3. Salathe, M. Regulation of mammalian ciliary beating. *Annu Rev Physiol* **69**, 401-422 (2007).
4. Voronina, V.A., Takemaru, K., Treuting, P., Love, D., Grubb, B.R., *et al.* Inactivation of Chibby affects function of motile airway cilia. *J Cell Biol* **185**, 225-233 (2009).
5. Ibanez-Tallon, I., Pagenstecher, A., Fliegauf, M., Olbrich, H., Kispert, A., *et al.* Dysfunction of axonemal dynein heavy chain Mdnah5 inhibits ependymal flow and reveals a novel mechanism for hydrocephalus formation. *Hum Mol Genet* **13**, 2133-2141 (2004).
6. Banizs, B., Pike, M.M., Millican, C.L., Ferguson, W.B., Komlosi, P., *et al.* Dysfunctional cilia lead to altered ependyma and choroid plexus function, and result in the formation of hydrocephalus. *Development* **132**, 5329-5339 (2005).
7. Lechtreck, K.F., Delmotte, P., Robinson, M.L., Sanderson, M.J. & Witman, G.B. Mutations in Hydin impair ciliary motility in mice. *J Cell Biol* **180**, 633-643 (2008).
8. Davy, B.E. & Robinson, M.L. Congenital hydrocephalus in hy3 mice is caused by a frameshift mutation in Hydin, a large novel gene. *Hum Mol Genet* **12**, 1163-1170 (2003).
9. Simons, M. & Mlodzik, M. Planar cell polarity signaling: from fly development to human disease. *Annu Rev Genet* **42**, 517-540 (2008).
10. Strutt, D.I., Weber, U. & Mlodzik, M. The role of RhoA in tissue polarity and Frizzled signalling. *Nature* **387**, 292-295 (1997).
11. Wang, Y. & Nathans, J. Tissue/planar cell polarity in vertebrates: new insights and new questions. *Development* **134**, 647-658 (2007).
12. Kibar, Z., Vogan, K.J., Groulx, N., Justice, M.J., Underhill, D.A., *et al.* Ltap, a mammalian homolog of Drosophila Strabismus/Van Gogh, is altered in the mouse neural tube mutant Loop-tail. *Nat Genet* **28**, 251-255 (2001).
13. Curtin, J.A., Quint, E., Tsipouri, V., Arkell, R.M., Cattanach, B., *et al.* Mutation of Celsr1 disrupts planar polarity of inner ear hair cells and causes severe neural tube defects in the mouse. *Curr Biol* **13**, 1129-1133 (2003).
14. Montcouquiol, M., Sans, N., Huss, D., Kach, J., Dickman, J.D., *et al.* Asymmetric localization of Vangl2 and Fz3 indicate novel mechanisms for planar cell polarity in mammals. *J Neurosci* **26**, 5265-5275 (2006).
15. Ravni, A., Qu, Y., Goffinet, A.M. & Tissir, F. Planar Cell Polarity Cadherin Celsr1 Regulates Skin Hair Patterning in the Mouse. *J Invest Dermatol* (2009).
16. Guo, N., Hawkins, C. & Nathans, J. Frizzled6 controls hair patterning in mice. *Proc Natl Acad Sci U S A* **101**, 9277-9281 (2004).
17. Devenport, D. & Fuchs, E. Planar polarization in embryonic epidermis orchestrates global asymmetric morphogenesis of hair follicles. *Nat Cell Biol* **10**, 1257-1268 (2008).
18. Shima, Y., Kawaguchi, S.Y., Kosaka, K., Nakayama, M., Hoshino, M., *et al.* Opposing roles in neurite growth control by two seven-pass transmembrane cadherins. *Nat Neurosci* (2007).
19. Tissir, F., Bar, I., Jossin, Y. & Goffinet, A.M. Protocadherin Celsr3 is crucial in axonal tract development. *Nat Neurosci* **8**, 451-457 (2005).
20. Wang, Y., Thekdi, N., Smallwood, P.M., Macke, J.P. & Nathans, J. Frizzled-3 is required for the development of major fiber tracts in the rostral CNS. *J Neurosci* **22**, 8563-8573 (2002).

21. Park, T.J., Mitchell, B.J., Abitua, P.B., Kintner, C. & Wallingford, J.B. Dishevelled controls apical docking and planar polarization of basal bodies in ciliated epithelial cells. *Nat Genet* **40**, 871-879 (2008).
22. Park, T.J., Haigo, S.L. & Wallingford, J.B. Ciliogenesis defects in embryos lacking inturned or fuzzy function are associated with failure of planar cell polarity and Hedgehog signaling. *Nat Genet* **38**, 303-311 (2006).
23. Zhou, L., Bar, I., Achouri, Y., Campbell, K., De Backer, O., *et al.* Early forebrain wiring: genetic dissection using conditional Celsr3 mutant mice. *Science* **320**, 946-949 (2008).
24. Shima, Y., Copeland, N.G., Gilbert, D.J., Jenkins, N.A., Chisaka, O., *et al.* Differential expression of the seven-pass transmembrane cadherin genes Celsr1-3 and distribution of the Celsr2 protein during mouse development. *Dev Dyn* **223**, 321-332 (2002).
25. Tissir, F., De-Backer, O., Goffinet, A.M. & Lambert de Rouvroit, C. Developmental expression profiles of Celsr (Flamingo) genes in the mouse. *Mech Dev* **112**, 157-160 (2002).
26. Formstone, C.J. & Little, P.F. The flamingo-related mouse Celsr family (Celsr1-3) genes exhibit distinct patterns of expression during embryonic development. *Mech Dev* **109**, 91-94 (2001).
27. Town, T., Breunig, J.J., Sarkisian, M.R., Spilianakis, C., Ayoub, A.E., *et al.* The stumpy gene is required for mammalian ciliogenesis. *Proc Natl Acad Sci U S A* **105**, 2853-2858 (2008).
28. Mirzadeh, Z., Merkle, F.T., Soriano-Navarro, M., Garcia-Verdugo, J.M. & Alvarez-Buylla, A. Neural stem cells confer unique pinwheel architecture to the ventricular surface in neurogenic regions of the adult brain. *Cell Stem Cell* **3**, 265-278 (2008).
29. Danilov, A.I., Gomes-Leal, W., Ahlenius, H., Kokaia, Z., Carlemalm, E., *et al.* Ultrastructural and antigenic properties of neural stem cells and their progeny in adult rat subventricular zone. *Glia* **57**, 136-152 (2009).
30. Sawamoto, K., Wichterle, H., Gonzalez-Perez, O., Cholfin, J.A., Yamada, M., *et al.* New neurons follow the flow of cerebrospinal fluid in the adult brain. *Science* **311**, 629-632 (2006).
31. Spassky, N., Merkle, F.T., Flames, N., Tramontin, A.D., Garcia-Verdugo, J.M., *et al.* Adult ependymal cells are postmitotic and are derived from radial glial cells during embryogenesis. *J Neurosci* **25**, 10-18 (2005).
32. Boisvieux-Ulrich, E. & Sandoz, D. Determination of ciliary polarity precedes differentiation in the epithelial cells of quail oviduct. *Biol Cell* **72**, 3-14 (1991).
33. Dawe, H.R., Farr, H. & Gull, K. Centriole/basal body morphogenesis and migration during ciliogenesis in animal cells. *J Cell Sci* **120**, 7-15 (2007).
34. Mitchell, B., Jacobs, R., Li, J., Chien, S. & Kintner, C. A positive feedback mechanism governs the polarity and motion of motile cilia. *Nature* **447**, 97-101 (2007).
35. Boisvieux-Ulrich, E., Laine, M.C. & Sandoz, D. Cytochalasin D inhibits basal body migration and ciliary elongation in quail oviduct epithelium. *Cell Tissue Res* **259**, 443-454 (1990).
36. Boisvieux-Ulrich, E., Laine, M.C. & Sandoz, D. In vitro effects of benzodiazepines on ciliogenesis in the quail oviduct. *Cell Motil Cytoskeleton* **8**, 333-344 (1987).
37. Marshall, W.F. The cell biological basis of ciliary disease. *J Cell Biol* **180**, 17-21 (2008).
38. Goebbels, S., Bormuth, I., Bode, U., Hermanson, O., Schwab, M.H., *et al.* Genetic targeting of principal neurons in neocortex and hippocampus of NEX-Cre mice. *Genesis* **44**, 611-621 (2006).
39. Jones, C., Roper, V.C., Foucher, I., Qian, D., Banizs, B., *et al.* Ciliary proteins link basal body polarization to planar cell polarity regulation. *Nat Genet* **40**, 69-77 (2008).
40. Wang, Y., Guo, N. & Nathans, J. The role of Frizzled3 and Frizzled6 in neural tube closure and in the planar polarity of inner-ear sensory hair cells. *J Neurosci* **26**, 2147-2156 (2006).
41. Ross, A.J., May-Simera, H., Eichers, E.R., Kai, M., Hill, J., *et al.* Disruption of Bardet-Biedl syndrome ciliary proteins perturbs planar cell polarity in vertebrates. *Nat Genet* **37**, 1135-1140 (2005).

42. Mirzadeh, Z., Han, Y.G., Soriano-Navarro, M., Garcia-Verdugo, J.M. & Alvarez-Buylla, A. Cilia organize ependymal planar polarity. *J Neurosci* **30**, 2600-2610 (2010).
43. Wong, L.L. & Adler, P.N. Tissue polarity genes of Drosophila regulate the subcellular location for prehair initiation in pupal wing cells. *J Cell Biol* **123**, 209-221 (1993).
44. Chen, J., Knowles, H.J., Hebert, J.L. & Hackett, B.P. Mutation of the mouse hepatocyte nuclear factor/forkhead homologue 4 gene results in an absence of cilia and random left-right asymmetry. *J Clin Invest* **102**, 1077-1082 (1998).
45. Brody, S.L., Yan, X.H., Wuerffel, M.K., Song, S.K. & Shapiro, S.D. Ciliogenesis and left-right axis defects in forkhead factor HFH-4-null mice. *Am J Respir Cell Mol Biol* **23**, 45-51 (2000).
46. Pan, J., You, Y., Huang, T. & Brody, S.L. RhoA-mediated apical actin enrichment is required for ciliogenesis and promoted by Foxj1. *J Cell Sci* **120**, 1868-1876 (2007).
47. Gomperts, B.N., Gong-Cooper, X. & Hackett, B.P. Foxj1 regulates basal body anchoring to the cytoskeleton of ciliated pulmonary epithelial cells. *J Cell Sci* **117**, 1329-1337 (2004).
48. Ropper, A.H. & Brown, R.H. *Adams and Victor's Principles of Neurology* (McGraw Hill, 2005).
49. Sharma, N., Berbari, N.F. & Yoder, B.K. Ciliary dysfunction in developmental abnormalities and diseases. *Curr Top Dev Biol* **85**, 371-427 (2008).
50. Tissir, F. & Goffinet, A.M. Expression of planar cell polarity genes during development of the mouse CNS. *Eur J Neurosci* **23**, 597-607 (2006).

Supplementary Information Guide

Supplementary Fig. 1: Targeted insertion of LacZ into Celsr2 locus.

Supplementary Fig. 2: The subcommissural organ (SCO) develops normally in *Celsr2* mutant mice.

Supplementary Fig. 3: Choroid plexus displays normal cilia in *Celsr2* and *Celsr2+3* mutant mice.

Supplementary Fig. 4: Ependymal cells differentiate normally in Celsr2 and Celsr2+3 mutant mice.

Supplementary Fig. 5: Ependymal cilia have normal ultrastructure.

Supplementary Fig. 6: Normal distribution of Z0-1.

Supplementary Movies 1-4: Cilia beat exhibits two types of movements.

Supplementary Movie 5: Movement of latex beads in lateral ventricle of WT and Celsr2 mutant tissue.

Supplementary Table 1: RT-PCR analysis of the *Celsr2* recombinant mRNA.

Supplementary Table 2: Comparison of bead track orientation using circular statistics, Watson's U^2 test.

Supplementary text: Partial sequence of mutant *Celsr2-LacZ-Neo* cDNA.

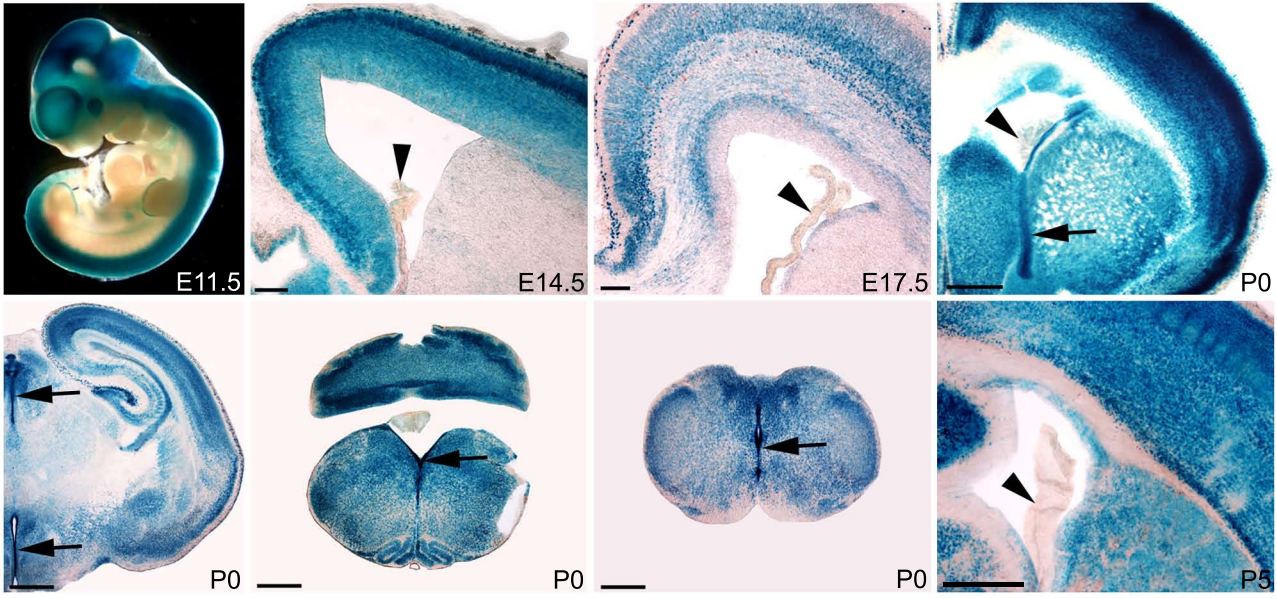
E11.5
E14.5
E17.5
P0
P0
P0
P0
P5

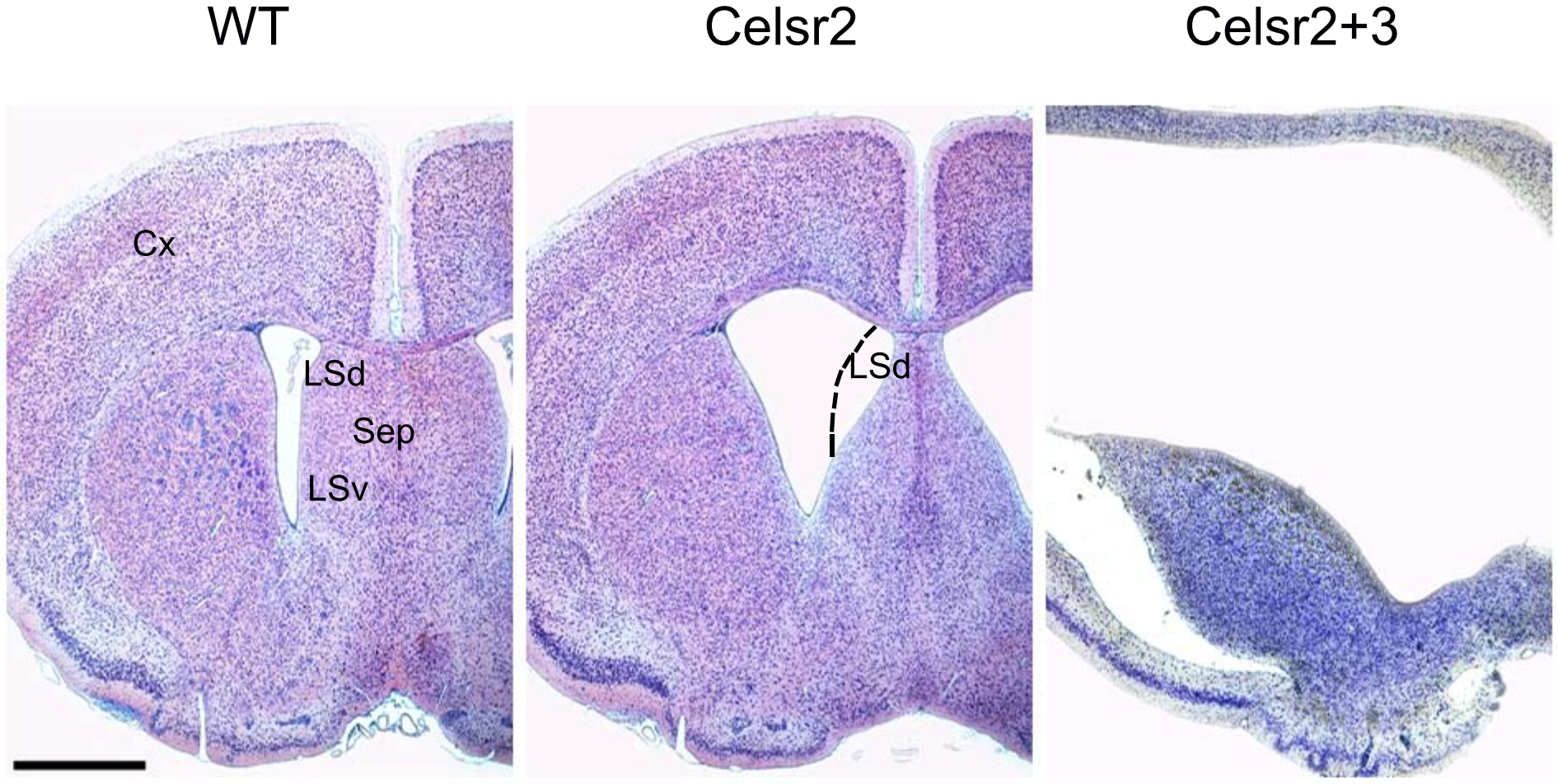
WT
Celsr2
Celsr2+3
Cx
LSd
Sep
LSv
LSd

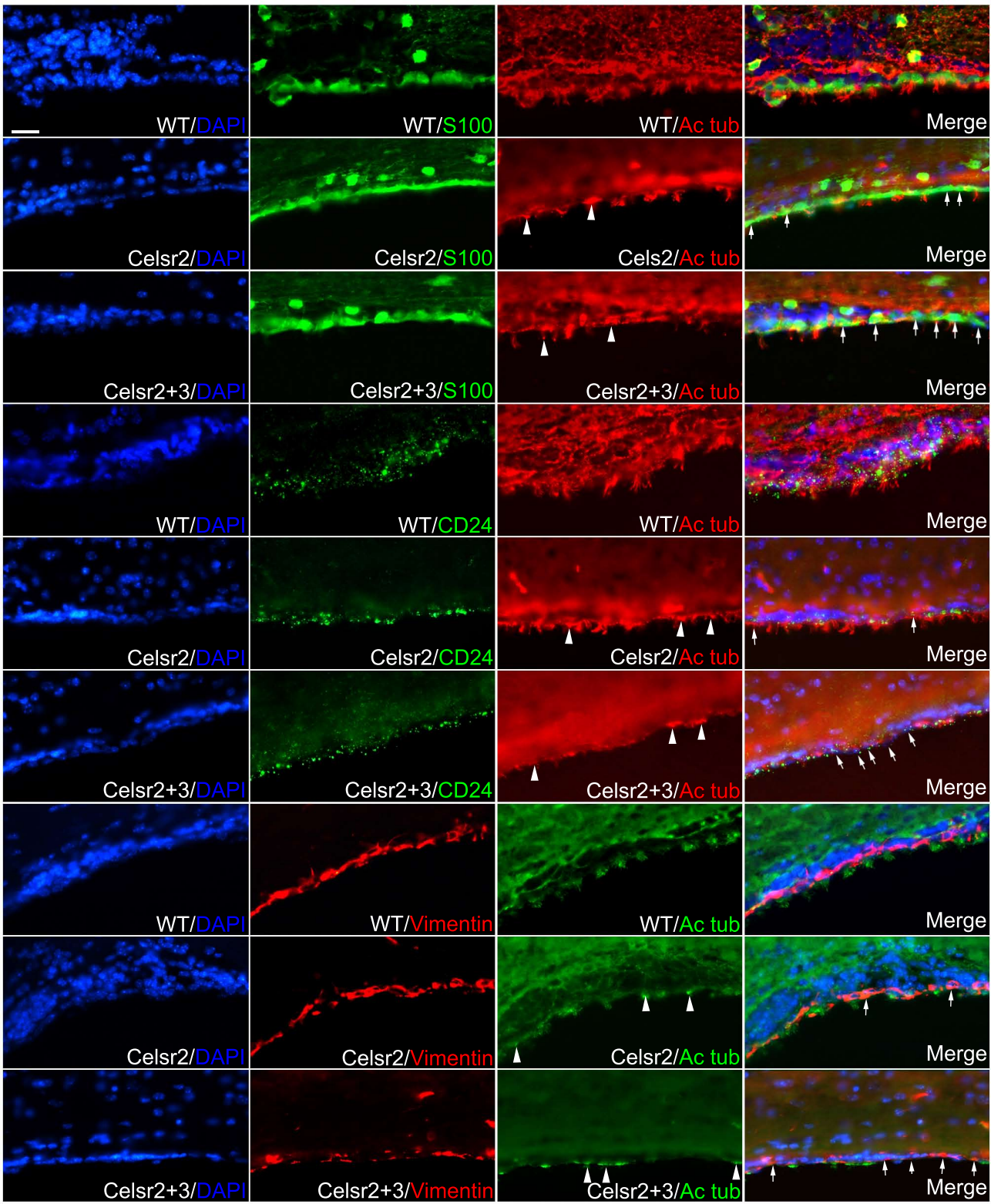
WT/DAPI
WT/S100
WT/Ac tub
Merge
Celsr2/DAPI
Celsr2/S100
Cels2/Ac tub
Merge
Celsr2+3/DAPI
Celsr2+3/S100
Celsr2+3/Ac tub
Merge
WT/DAPI
WT/CD24
WT/Ac tub
Merge
Celsr2/DAPI
Celsr2/CD24
Celsr2/Ac tub
Merge
Celsr2+3/DAPI
Celsr2+3/CD24
Celsr2+3/Ac tub
Merge
WT/DAPI
WT/Vimentin
WT/Ac tub
Merge
Celsr2/DAPI
Celsr2/Vimentin
Celsr2/Ac tub
Merge
Celsr2+3/DAPI
Celsr2+3/Vimentin
Celsr2+3/Ac tub
Merge

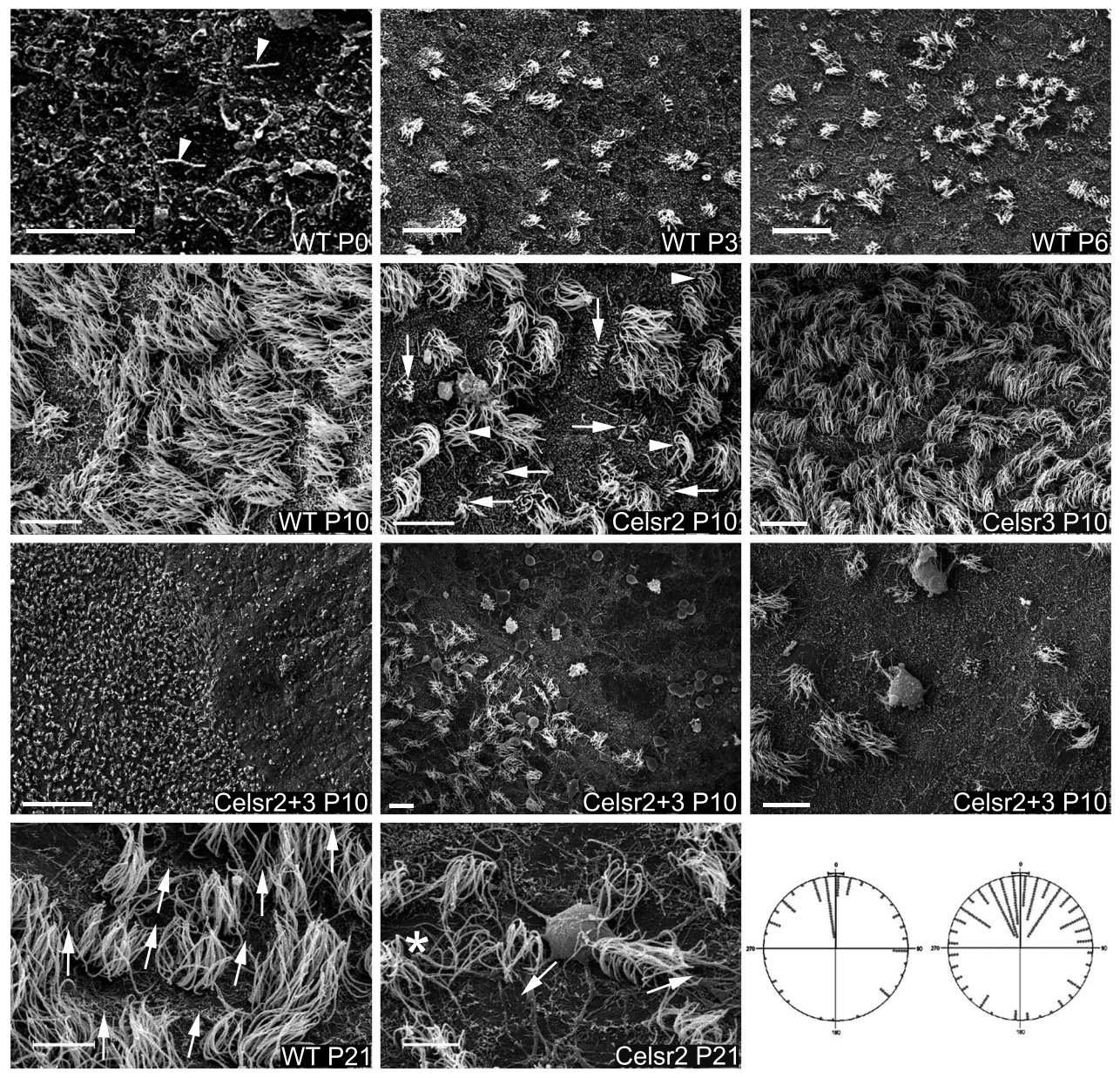
WT P0
WT P3
WT P6
WT P10
Celsr2 P10
Celsr3 P10
Celsr2+3 P10
Celsr2+3 P10
Celsr2+3 P10
WT P21
Celsr2 P21
0
90
180
270
0
90
180
270

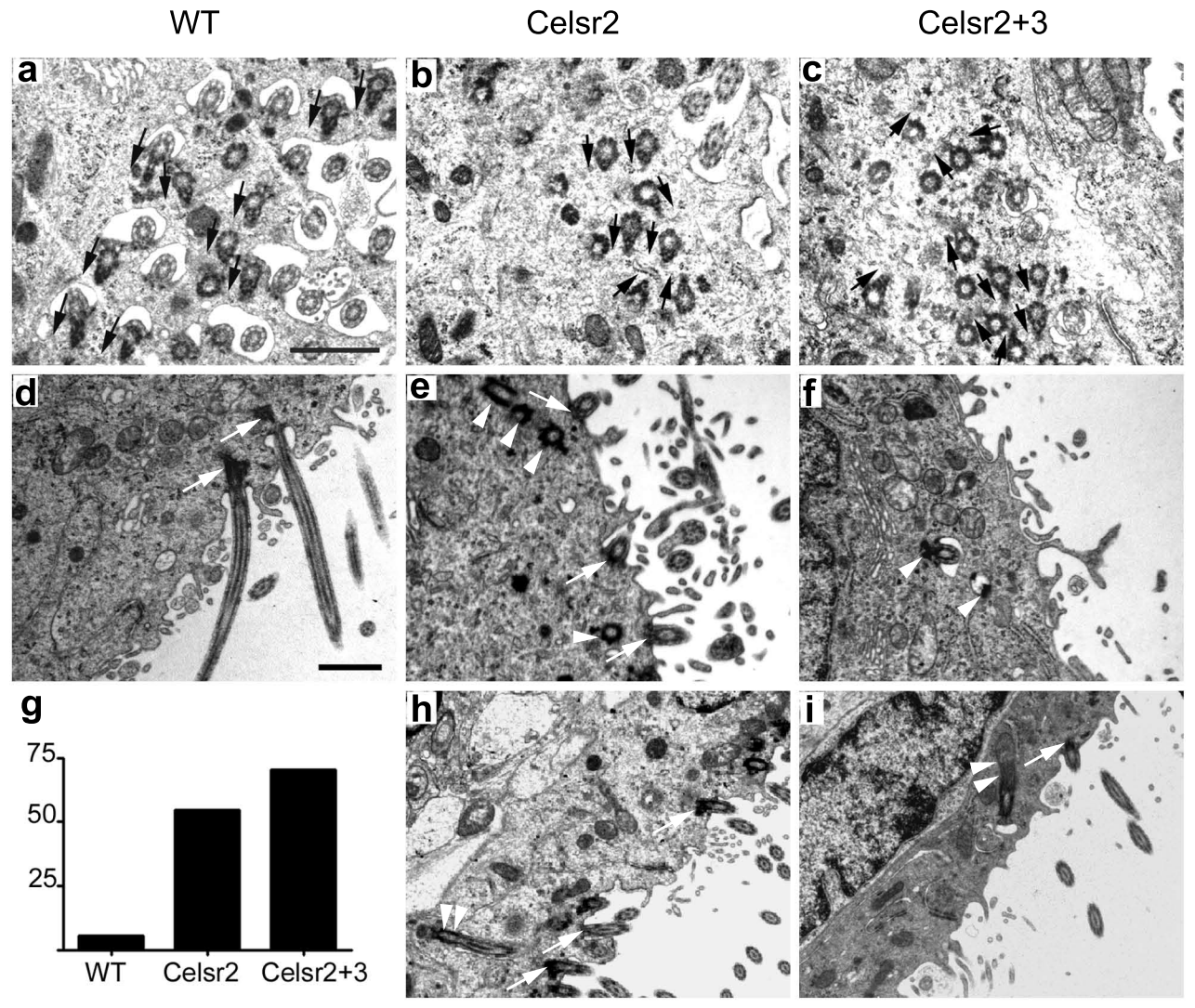
WT
Celsr2
Celsr2+3
a
b
c
d
e
f
g
h
i
75
50
25
WT
Celsr2
Celsr2+3

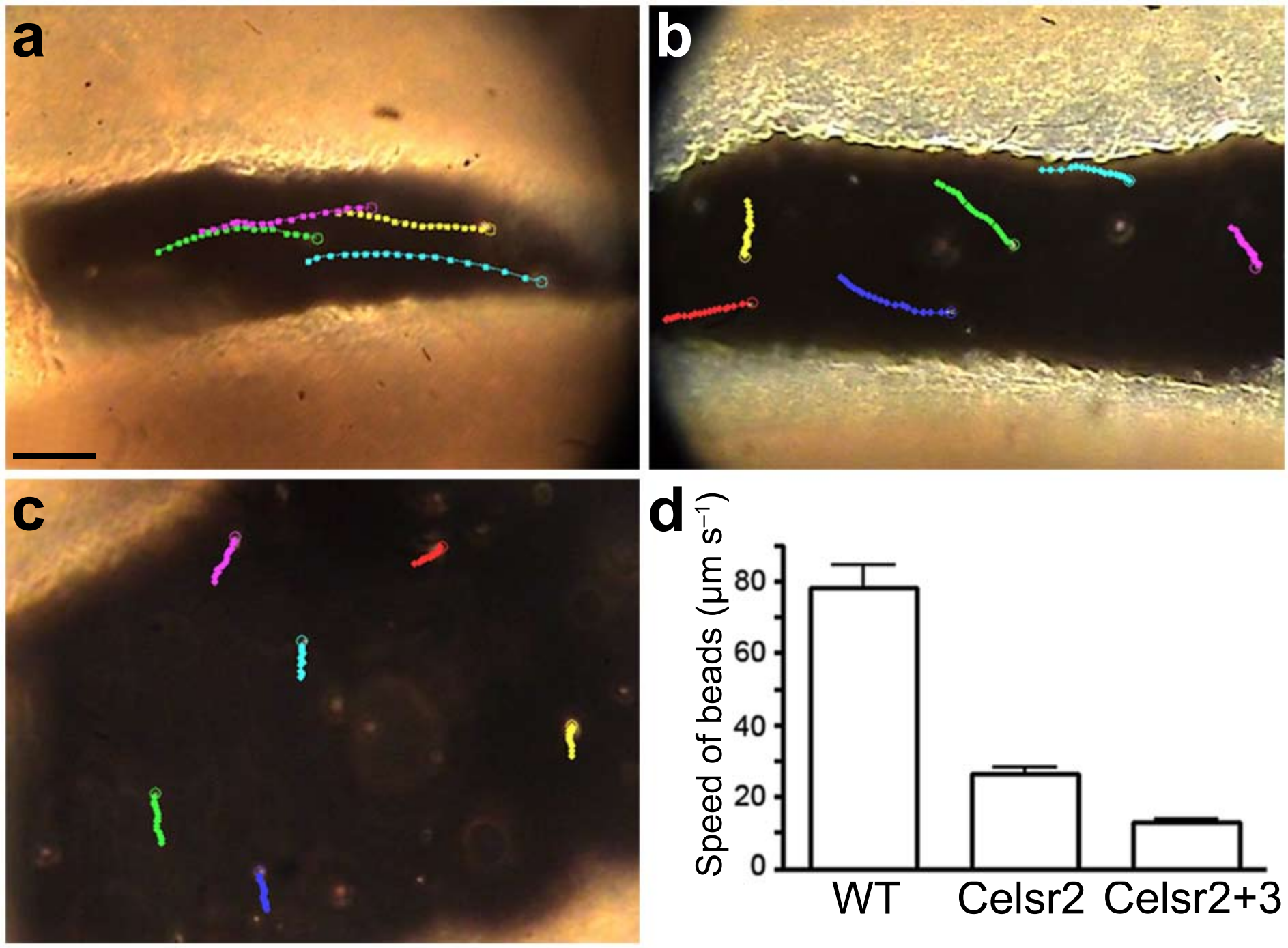
a
b
c
d
Speed of beads (μm s−1)
80
60
40
20
0
WT
Celsr2
Celsr2+3

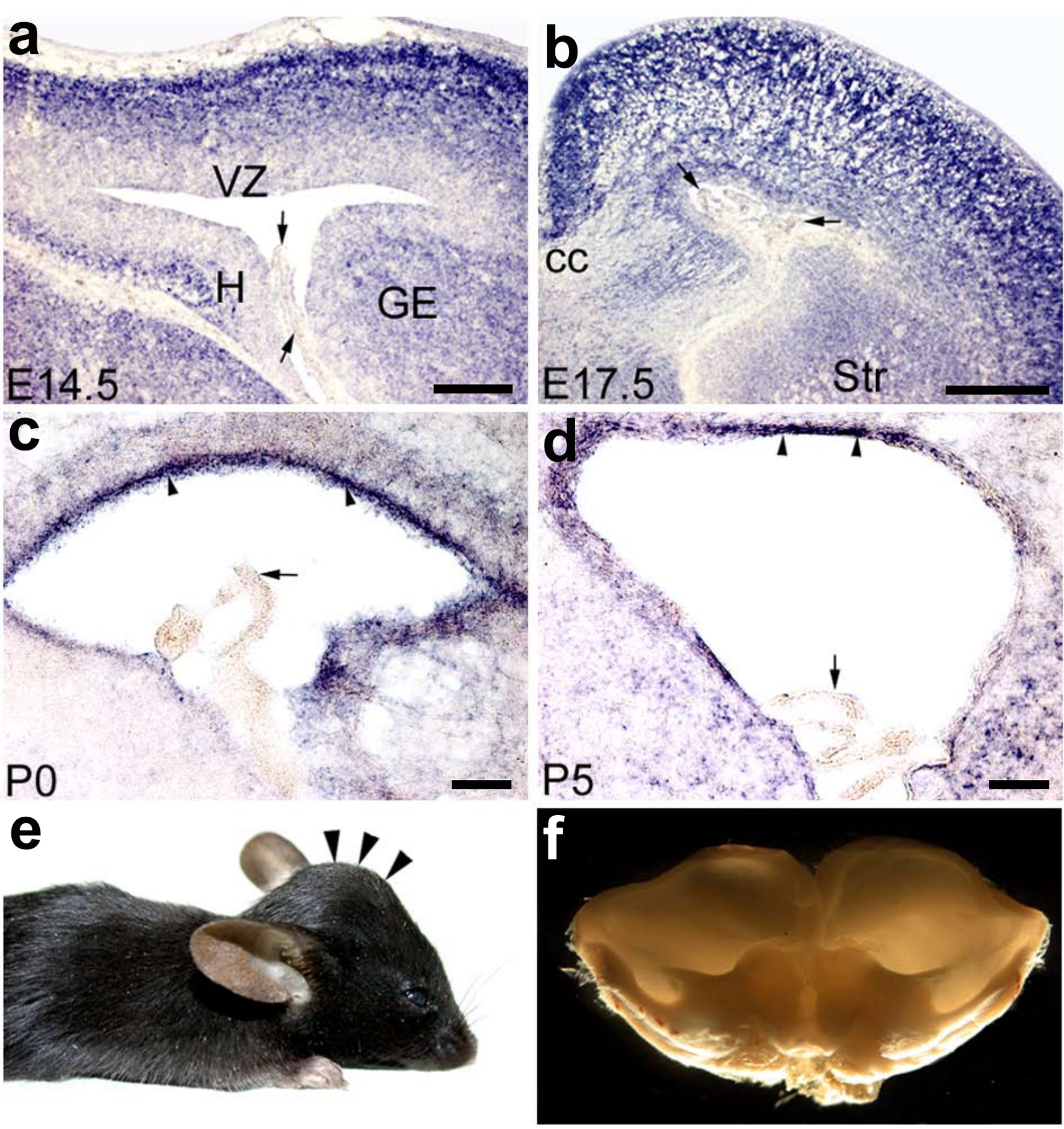
a
VZ
H
GE
E14.5
b
cc
E17.5
Str
c
P0
d
P5
e
f

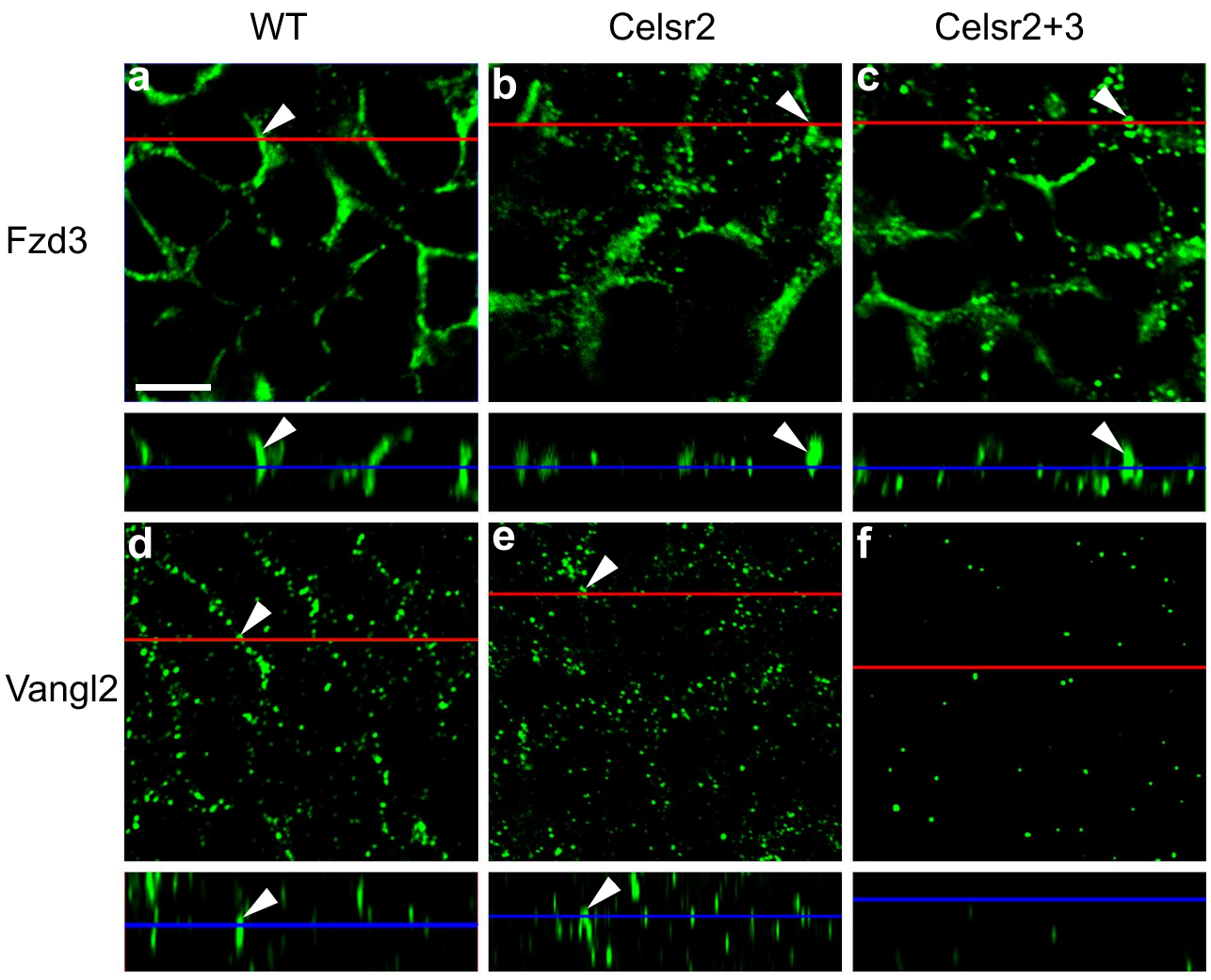
WT
Celsr2
Celsr2+3
Fzd3
Vangl2
a
b
c
d
e
f